

# A generalized multiscale finite element method for neutron transport problems in $SP_3$ approximation

Aleksandr O. Vasilev<sup>a,\*</sup>, Denis A. Spiridonov<sup>a</sup>, Alexander V. Avvakumov<sup>b</sup>

<sup>a</sup>*North-Eastern Federal University, 58, Belinskogo, Yakutsk, Russia*

<sup>b</sup>*National Research Center Kurchatov Institute, 1, Sq. Academician Kurchatov, Moscow, Russia*

---

## Abstract

The  $SP_3$  approximation of the neutron transport equation allows improving the accuracy for both static and transient simulations for reactor core analysis compared with the neutron diffusion theory. Besides, the  $SP_3$  calculation costs are much less than higher order transport methods ( $S_N$  or  $P_N$ ). Another advantage of the  $SP_3$  approximation is a similar structure of equations that is used in the diffusion method. Therefore, there is no difficulty to implement the  $SP_3$  solution option to the multi-group neutron diffusion codes.

In this paper, we attempt to employ a model reduction technique based on the multiscale method for neutron transport equation in  $SP_3$  approximation. The proposed method is based on the use of a generalized multiscale finite element method (GMSFEM). The main idea is to create multiscale basis functions that can be used to effectively solve on a coarse grid. From calculation results, we obtain that multiscale basis functions can properly take into account the small-scale characteristics of the medium and provide accurate solutions. The application of the  $SP_3$  methodology based on solution of the  $\lambda$ -spectral problems has been tested for the some reactor benchmarks. The results calculated with the GMSFEM are compared with the reference transport calculation results.

*Keywords:* neutron transport equation,  $SP_3$  approximation, eigenvalues, multiscale simulation, generalized multiscale finite element method, GMSFEM

---

## 1. Introduction

## 2. Problem statement

Let us consider the symmetric form of the  $SP_3$  equation for the neutron flux. The neutron dynamics is considered in the limited convex two-dimensional or

---

\*Corresponding author

Email addresses: [haska87@gmail.com](mailto:haska87@gmail.com) (Aleksandr O. Vasilev), [d.stalnov@mail.ru](mailto:d.stalnov@mail.ru) (Denis A. Spiridonov), [Avvakumov2009@rambler.ru](mailto:Avvakumov2009@rambler.ru) (Alexander V. Avvakumov)

three-dimensional area  $\Omega$  ( $\mathbf{x} = \{x_1, \dots, x_d\} \in \Omega$ ,  $d = 2, 3$ ) with boundary  $\partial\Omega$ . The neutron transport is described by the system of equations

$$\begin{aligned} & \frac{1}{v_g} \frac{\partial \phi_{0,g}}{\partial t} - \frac{2}{v_g} \frac{\partial \phi_{2,g}}{\partial t} - \nabla \cdot D_{0,g} \nabla \phi_{0,g} + \Sigma_{r,g} \phi_{0,g} - 2\Sigma_{r,g} \phi_{2,g} \\ & = (1 - \beta) \chi_{n,g} S_n + S_{s,g} + \chi_{d,g} S_d, \\ & - \frac{2}{v_g} \frac{\partial \phi_{0,g}}{\partial t} + \frac{9}{v_g} \frac{\partial \phi_{2,g}}{\partial t} - \nabla \cdot D_{2,g} \nabla \phi_{2,g} + 5\Sigma_{t,g} + 4\Sigma_{r,g} \phi_{2,g} - 2\Sigma_{r,g} \phi_{0,g} \\ & = -2(1 - \beta) \chi_{n,g} S_n - 2S_{s,g} - 2\chi_{d,g} S_d, \end{aligned} \quad (1)$$

where

$$\begin{aligned} S_n &= \sum_{g'=1}^G \nu \Sigma_{f,g'} \phi_{g'}, \quad S_{s,g} = \sum_{g \neq g'=1}^G \Sigma_{s,g' \rightarrow g} \phi_{g'}, \quad S_d = \sum_{m=1}^M \lambda_m c_m, \\ \phi_{0,g} &= \phi_g + 2\phi_{2,g}, \quad D_{0,g} = \frac{1}{3\Sigma_{tr,g}}, \quad D_{2,g} = \frac{9}{7\Sigma_{t,g}}, \quad g = 1, 2, \dots, G. \end{aligned}$$

Here  $G$  — number of energy groups,  $\phi_g(\mathbf{x}, t)$  — scalar flux,  $\phi_{0,g}(\mathbf{x}, t)$  — pseudo 0th moment of angular flux,  $\phi_{2,g}(\mathbf{x}, t)$  — second moment of angular flux,  $\Sigma_{t,g}(\mathbf{x}, t)$  — total cross-section,  $\Sigma_{tr,g}(\mathbf{x}, t)$  — transport cross-section,  $\Sigma_{r,g}(\mathbf{x}, t)$  — removal cross-section,  $\Sigma_{s,g' \rightarrow g}(\mathbf{x}, t)$  — scattering cross-section,  $\chi_g$  — spectra of neutrons,  $\nu \Sigma_{f,g}(\mathbf{x}, t)$  — generation cross-section,  $c_m(\mathbf{x}, t)$  — density of sources of delayed neutrons,  $\lambda_m$  — decay constant of sources of delayed neutrons,  $M$  — number of types of delayed neutrons.

The density of sources of delayed neutrons is described by the equations

$$\frac{\partial c_m}{\partial t} + \lambda_m c_m = \beta_m S_n, \quad m = 1, 2, \dots, M, \quad (2)$$

where  $\beta_m$  is the fraction of delayed neutrons of  $m$ -type, and

$$\beta = \sum_{m=1}^M \beta_m.$$

The Marshak-type conditions are set at the boundary of the area  $\partial\Omega$

$$\begin{aligned} \begin{bmatrix} J_{0,g}(\mathbf{x}) \\ J_{2,g}(\mathbf{x}) \end{bmatrix} &= \begin{bmatrix} \frac{1}{2} & -\frac{3}{8} \\ -\frac{3}{8} & \frac{21}{8} \end{bmatrix} \begin{bmatrix} \phi_{0,g}(\mathbf{x}) \\ \phi_{2,g}(\mathbf{x}) \end{bmatrix}, \\ J_{i,g}(\mathbf{x}) &= -D_{i,g} \nabla \phi_{i,g}(\mathbf{x}), \quad i = 0, 2. \end{aligned} \quad (3)$$

System of equations (1) and (2) is supplemented with boundary conditions (3) and corresponding initial conditions

$$\begin{aligned} \phi_g(\mathbf{x}, 0) &= \phi_g^0(\mathbf{x}), \quad g = 1, 2, \dots, G, \\ c_m(\mathbf{x}, 0) &= c_m^0(\mathbf{x}), \quad m = 1, 2, \dots, M. \end{aligned} \quad (4)$$

We assume that at the initial time  $t = 0$ , the reactor is in steady-state critical condition.

**Discretization.** Let's discretize the boundary problem (1)-(4). Define a uniform grid

$$\omega = \{t^n = n\tau, \quad n = 0, 1, \dots, N, \quad \tau N = T\}$$

and use the next notations  $\phi_g^n = \phi_g(\mathbf{x}, t^n)$ ,  $c_m^n = c_m(\mathbf{x}, t^n)$ . We discretize the time derivatives of equation (1) using finite-difference scheme. We use a fully implicit scheme with time step  $\tau$  for the time approximation. For delayed neutron source equation, we use numerical-analytical method for the construction of approximations in time. The equation (2) in the equivalent form

$$\frac{\partial e^{\lambda_m t} c_m}{\partial t} = \beta_m e^{\lambda_m t} \sum_{g=1}^G \nu \Sigma_{fg} \phi_g, \quad m = 1, 2, \dots, M.$$

After integration over time interval  $[t^n, t^{n+1}]$  one can obtain

$$c_m^{n+1} = e^{-\lambda_m \tau} c_m^n + \beta_m \int_{t_n}^{t_{n+1}} e^{\lambda_m(t-t^{n+1})} \sum_{g=1}^G \nu \Sigma_{fg} \phi_g dt, \quad m = 1, 2, \dots, M. \quad (5)$$

When using the fully implicit scheme, we take the integrand on the right-hand side of (5) at  $t = t^{n+1}$ .

We use finite element method for the spatial approximation. Let  $H^1(\Omega)$  – Sobolev space,  $q \in H^1$ :  $q^2$  and  $|\nabla q|^2$  have a finite integral in  $\Omega$ . Using the integration by parts, we obtain the following variational formulation: let's find  $\phi_g^{n+1} \in V^G$  such that

$$\begin{aligned} & \int_{\Omega} \left( \frac{\phi_{0,g}^{n+1} - \phi_{0,g}^n}{v_g \tau} - \frac{2(\phi_{2,g}^{n+1} - \phi_{2,g}^n)}{v_g \tau} \right) q_g d\mathbf{x} - \int_{\Omega} D_{0,g} \nabla \phi_{0,g}^{n+1} \nabla q_g d\mathbf{x} \\ & + \int_{\partial\Omega} J_{0,g}^{n+1} q_g d\mathbf{s} + \int_{\Omega} (\Sigma_{r,g} \phi_{0,g}^{n+1} - 2\Sigma_{r,g} \phi_{2,g}^{n+1}) q_g d\mathbf{x} \\ & = \int_{\Omega} ((1-\beta)\chi_{n,g} S_n^{n+1} + S_{s,g}^{n+1} + \chi_{d,g} S_d^{n+1}) q_g d\mathbf{x}, \\ & \int_{\Omega} \left( -\frac{2(\phi_{0,g}^{n+1} - \phi_{0,g}^n)}{v_g \tau} + \frac{9(\phi_{2,g}^{n+1} - \phi_{2,g}^n)}{v_g \tau} \right) q_g d\mathbf{x} - \int_{\Omega} D_{2,g} \nabla \phi_{2,g}^{n+1} \nabla q_g d\mathbf{x} \\ & + \int_{\partial\Omega} J_{2,g}^{n+1} q_g d\mathbf{s} + \int_{\Omega} ((5\Sigma_{t,g} + 4\Sigma_{r,g}) \phi_{2,g}^{n+1} - 2\Sigma_{r,g} \phi_{0,g}^{n+1}) q_g d\mathbf{x} \\ & = \int_{\Omega} (-2(1-\beta)\chi_{n,g} S_n^{n+1} - 2S_{s,g}^{n+1} - 2\chi_{d,g} S_d^{n+1}) q_g d\mathbf{x}, \end{aligned} \quad (6)$$

where  $V^G = [H^1(\Omega)]^G$ .

Further, it's necessary to pass from the continuous variational problem (6) to the discrete problem. We introduce finite-dimensional space of finite elements  $V_h^G \subset V^G$  and formulate a discrete variational problem. We use standard linear

basis functions as basis functions to solve the problem on the fine grid. The problem is solving a system of linear algebraic equations

$$A_f \phi = b_f, \quad (7)$$

where the operator  $A_f$  corresponds to the bilinear form of equation, and the vector  $b_f$  corresponds to the linear form of equation (6).

### 3. Multiscale method

For the discretization on the coarse grid we use GMsFEM. We construct two grids: fine grid ( $\mathcal{T}_h$ ) and coarse grid ( $\mathcal{T}_H$ ) (see Figure 1). For multiscale basis construction, we define local domains  $\omega_i$ , where  $i = 1, \dots, N_v$  and  $N_v$  is the number of coarse grid nodes. We assume that  $\mathcal{T}_h$  is a refinement of  $\mathcal{T}_H$ , where  $h$  and  $H$  represent the fine and coarse grid sizes, respectively. We assume that the fine-scale grid  $\mathcal{T}_h$  is sufficiently fine to fully resolve the small-scale information of the domain while  $\mathcal{T}_H$  is a coarse grid containing many fine-scale features. A local domain  $\omega_i$  is obtained by the combining all the coarse cells around one vertex of the coarse grid.

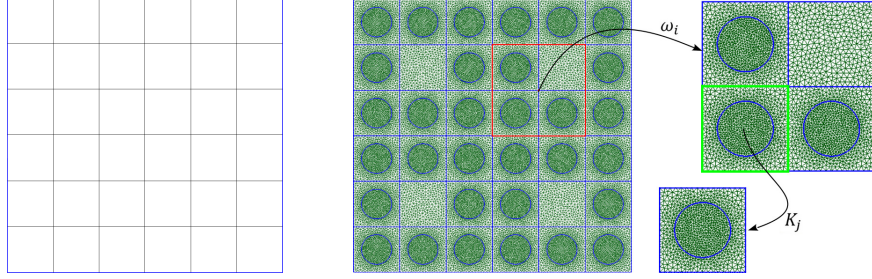


Figure 1: Coarse grid and local domain  $\omega_i$  with  $K_j$

We construct the multiscale function spaces

$$V_{\text{off}} = \text{span}\{y_j\}_{j=1}^N,$$

where  $N$  is the number of coarse basis functions. Each  $y_j$  is supported in local domain  $w_i$ .

Basis functions are designed to capture the multiscale features of the solution. Important multiscale features of the solution are incorporated into localized basis functions which contain information about the scales that are smaller (as well as larger) than the local numerical scale defined by the basis functions.

**Multiscale space.** The computation of basis functions use local spectral problems to reduce the dimension of the local problem. In order to construct conforming basis functions, we multiply eigenvectors related to dominant eigenvalues to the partition of unity functions. We use following spectral problem in  $\omega_i$

$$A\varphi^i = \lambda S\varphi^i, \quad (8)$$

where the elements of the matrices  $A = \{a_{ij}\}$  and  $S = \{s_{ij}\}$  are defined as follow

$$\begin{aligned} a_{ij} &= \int_{\omega_i} \\ s_{ij} &= \int_{\omega_i} \end{aligned} \quad (9)$$

Then, we choose eigenvectors corresponding to dominant  $M_i$  eigenvalues from (8) and use them to construct the multiscale basis functions.

As partition of unity functions, we use linear functions in each domain  $\omega_i$ . Partitions of unity are calculated in the domain  $K_j$  as a linear function from  $\Gamma$  to the vertex  $A$ , and 0 is assigned to the entire segment  $\Gamma$ , and at point  $A$  is assigned the value 1. Thus, we obtain a linear function from 0 to 1 over the entire domain  $K_j$ . Partitions of unity are shown in Figure 2. Domain  $K_j$  is one element from a coarse grid.

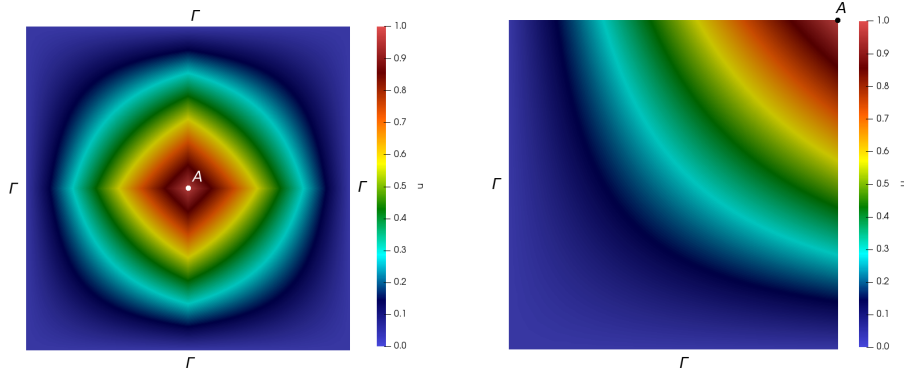


Figure 2: Partition of unity functions on the  $\omega_i$  (right) and  $K_j$  (left)

The multiscale space is defined as the span of  $y_i = \chi_i \varphi_k^i$ , where  $\chi_i$  is the usual nodal basis function for the node  $i$  (linear partition of unity functions). The number of bases can be different, the accuracy of the solution can be improved when we increase the number of bases.

**Coarse-scale approximation.** Next, we create the following matrix for each  $\omega_i$

$$R^i = [y_1, \dots, y_{M_i-1}, y_{M_i}].$$

and define the transition matrix from a fine grid to a coarse grid  $R$  to reduce the dimension of the problem

$$R = [R^1, R^2, \dots, R^{N_v}],$$

where  $N_v$  is the number of local domains  $\omega_i$ .

Then using the transition matrix  $R$  and fine grid system (7), we construct the coarse grid approximation

$$A_c \phi_c = b_c, \quad A_c = R A_f R^T \quad \text{and} \quad b_c = R b_f,$$

and using the coarse-scale solution  $\phi_c$ , we can reconstruct the fine grid solution

$$\phi_{ms} = R^T \phi_c.$$

#### 4. Numerical results

Numerical modeling of non-stationary tests is carried out in the transport  $SP_3$  approximation. Numerical results obtained by the finite element method and the generalized multiscale finite element method are analyzed and compared. The software has been written using the science library FEniCS. The SLEPc library has been used to solve spectral problems with asymmetric matrices.

At each time step, we calculate the integrated power as

$$P(t) = a \int_{\Omega} \sum_{g=1}^G \Sigma_{f,g} \phi_g d\mathbf{x},$$

where  $a$  is the normalization coefficient, that corresponds to a given value of the integrated power.

##### 4.1. One group test

Let's consider the 2D test problem for small PWR reactor ( $\Omega$  — reactor core area). The geometrical model of the small PWR reactor core is presented in Fig.3. The diameter of the fuel rod is 0.82 cm, the cell width is 1.26 cm. Neutronics constants in the common notations are given in Table 1. There are two types of cassettes, with fuel 1%  $UO_2$  and 2%  $UO_2$ . The following delayed neutrons parameters are used:  $\beta = 6.5 \cdot 10^{-3}$ ,  $\lambda = 0.08 \text{ s}^{-1}$  and  $v = 5 \cdot 10^5 \text{ cm/s}$ . The reflective boundary condition is set at the boundary of the domain.

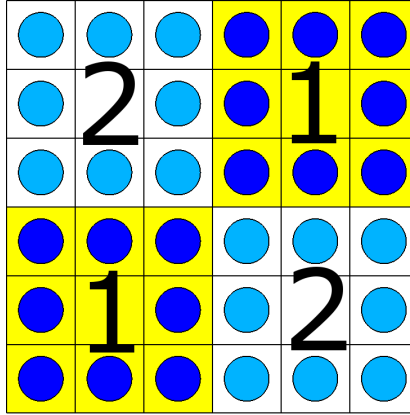


Figure 3: Geometrical model of the small PWR-2D reactor core

The coarse grid contains 49 vertices. The fine grid contains 115891 vertices. The calculation goes up to time  $T = 0.4$  sec. The time step for both grids is

$\tau = 0.001$ . We take a fine-grid solution as an exact solution. The initial value of  $K_{eff}$  is 1.18398.

Let's define the next scenario of the process:

- Solve the  $\lambda$ -spectral problem;
- As the initial condition, take the solution of the  $\lambda$ -spectral problem;
- At time  $t = 0.1$  sec, change the removal cross-section  $\Sigma_r$  for fuel in zone 1 by +2% (simulation of immersion of control rods);
- At time  $t = 0.3$  sec, change the removal cross-section  $\Sigma_r$  for fuel in zone 1 by -3% (simulation of withdrawal of control rods).

Table 1: Neutronics constants for small PWR-2D.

Material	1		2	
	coolant	fuel	coolant	fuel
$D$	3.4473872E-01	7.7002585E-01	3.1679441E-01	8.0236505E-01
$\Sigma_t$	9.6691584E-01	4.3288590E-01	1.0522071E+00	4.1543850E-01
$\Sigma_r$	5.3858400E-03	8.9337900E-02	6.0670900E-03	6.6279500E-02
$\Sigma_f$	0.0	5.4731800E-02	0.0	3.3377700E-02
$\nu$	0.0	2.44844862	0.0	2.45482762

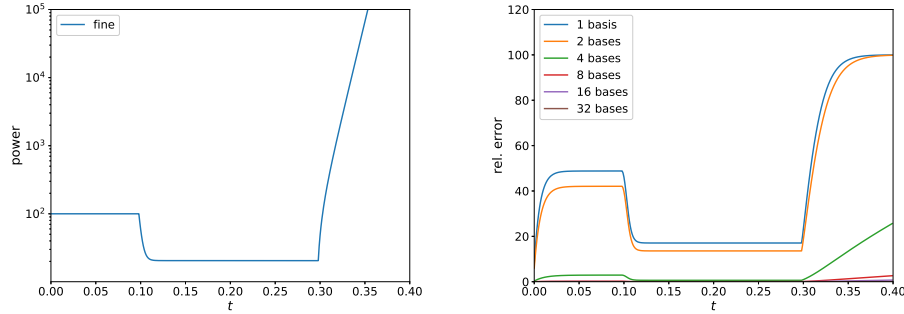


Figure 4: Integral power (fine grid) and relative errors (%) of the multiscale solution power.

The integral power for the fine grid and the relative errors (%) of the integral powers are shown in Figure 4. When using 4 or less multiscale basis functions, the error is more than 10% and for using 16 or more multiscale basis functions, the error it does not exceed 1%.

Figures 5, 6 show the relative  $L_2$  and  $H_1$  errors of the multiscale solution vs. time for a different number of multiscale basis functions. The numerical

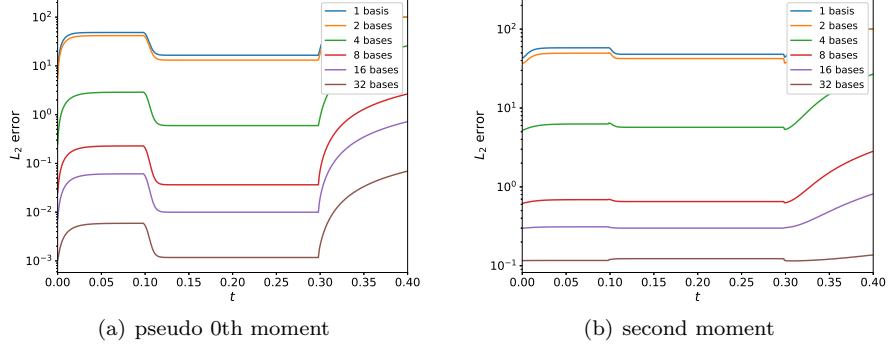


Figure 5: Relative  $L_2$  errors (%) of the multiscale solution of angular flux

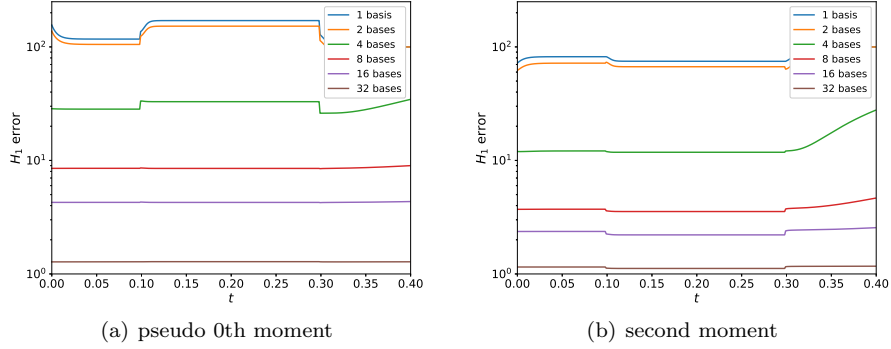


Figure 6: Relative  $H_1$  errors (%) of the multiscale solution of angular flux

results show good convergence provided that we take a sufficient number of the multiscale basis functions.

Table 2 shows the relative  $L_2$  and  $H_1$  errors at final time for a different number of the multiscale basis functions. For example, when we use 16 multiscale basis functions, we obtain 0.71% for  $L_2$  error and 4.34% for  $H_1$  error for pseudo 0th moment of angular flux. And the relative errors for second moment of angular flux are 0.81% for  $L_2$  and 2.56% for  $H_1$ . Calculations indicate that it is necessary to make use of 16 or more multiscale basis functions. The fine-grid solution and the multiscale solutions for a different number of bases (on each local domain  $\omega_i$ ) for pseudo 0th moment of angular flux at the final time are shown in Figure 7.

#### 4.2. two group test

The two-dimensional transport test TWIGL is considered. One fourth of the reactor core is modeled, the dimensions of that are 160x160 cm. Figure 8 shows the geometrical model of the core, where fuel assemblies of various types



Table 2: Relative  $L_2$  and  $H_1$  errors (%) of the solution at final time.

Bases	DOF	Pseudo 0th moment		Second moment		Calc time
		$L_2$ error	$H_1$ error	$L_2$ error	$H_1$ error	
1	49	99.97	99.99	99.97	99.99	0.03
2	98	99.83	99.90	99.84	99.90	0.05
4	196	25.61	34.38	26.65	27.64	0.10
8	392	2.64	8.99	2.80	4.65	0.35
16	784	0.71	4.34	0.81	2.56	1.15
32	1568	0.07	1.28	0.14	1.17	6.66
fine	115891	–	–	–	–	815.00

are shown. Neutronics constants in the common notations are given in Table 3. The fission spectrum for prompt and delayed neutrons is the same for the entire medium and  $\chi_1 = 1$ ,  $\chi_2 = 0$ . The following delayed neutrons parameters are used: one group of delayed neutrons with effective fraction  $\beta = 0.0075$  and decay constant  $\lambda = 0.08 \text{ s}^{-1}$ . Neutron velocity  $v_1 = 10^7 \text{ cm/s}$  and  $v_2 = 2 \cdot 10^5 \text{ cm/s}$ .

Table 3: Neutronics constants for TWIGL-2D.

Material	1	2	3
$\Sigma_{t,1}$	0.2481	0.2481	0.2644
$\Sigma_{t,2}$	0.9833	0.9833	0.7167
$\Sigma_{r,1}$	0.01	0.01	0.008
$\Sigma_{r,2}$	0.15	0.15	0.05
$\Sigma_{s,1 \rightarrow 2}$	0.01	0.01	0.01
$\Sigma_{s,1 \rightarrow 1}$	0.2281	0.2281	0.2464
$\Sigma_{s,2 \rightarrow 2}$	0.8333	0.8333	0.6667
$\nu_1 \Sigma_{f,1}$	0.007	0.007	0.003
$\nu_2 \Sigma_{f,2}$	0.2	0.2	0.06

We define the next scenario of the process:

- The  $\lambda$ -spectral problem is solved and the solution is taken as the initial condition;
- Calculation for the non-stationary model at the time range from 0 to 0.5 sec;
- An abrupt perturbation occurs in region 1 by changing the removal cross-section  $\Sigma_{r,2}$  by  $0.0035 \text{ cm}^{-1}$  at the zero moment of time.

The coarse grid contains 121 vertices. The fine grid contains 25921 vertices.

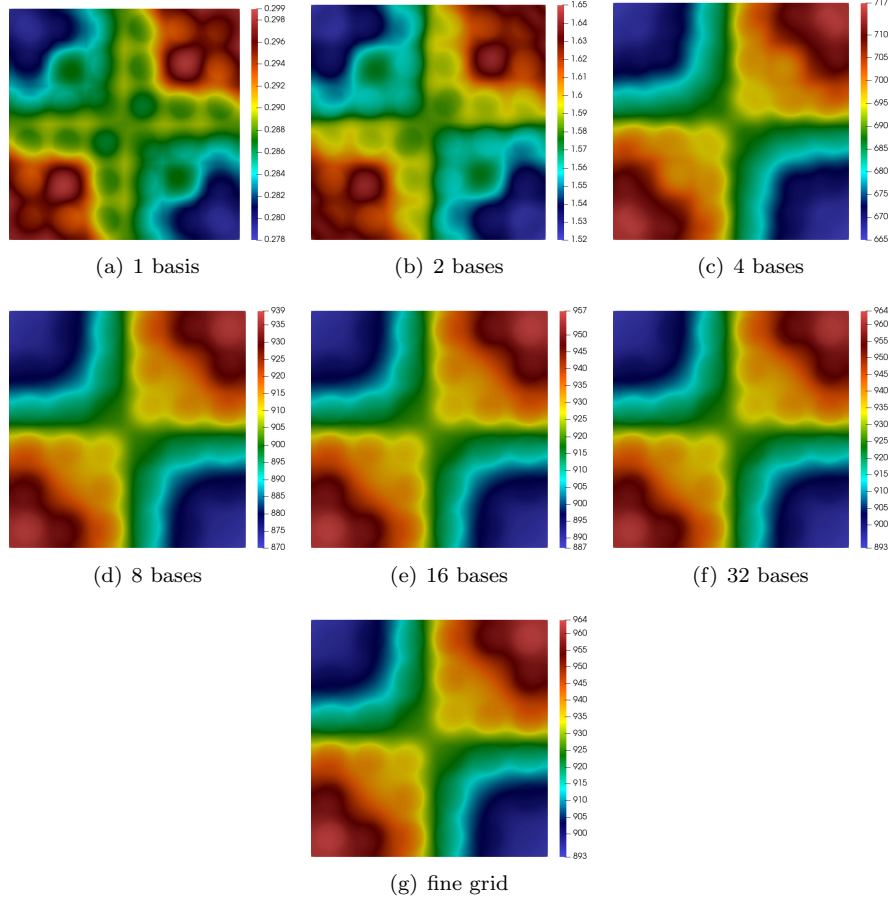


Figure 7: Fine-grid and multiscale solutions at final time for pseudo 0th moment of angular flux

The time step for both grids is  $\tau = 0.0001$ . As an exact solution, we take the fine-grid solution. The initial value of  $K_{eff}$  is 0.916075.

The integral power for the fine grid and relative errors (%) of integral powers are shown in Figure 9. When using using 4 or more multiscale basis functions, the error it does not exceed 3%.

In Figures 10, 6, we present relative  $L_2$  and  $H_1$  errors of the multiscale solution vs. time for different number of multiscale basis functions. Hereinafter, we use the following notation for multiscale solution:  $\phi_{ms0,1}$  — pseudo 0th moment of angular flux of fast (group 1) energy group;  $\phi_{ms2,1}$  — second moment of angular flux of fast energy group;  $\phi_{ms0,2}$  — pseudo 0th moment of angular flux of thermal (group 2) energy group;  $\phi_{ms2,2}$  — second moment of angular flux of thermal energy group. The numerical results show good convergence behaviour, provided that we take sufficient number of the multiscale basis functions.

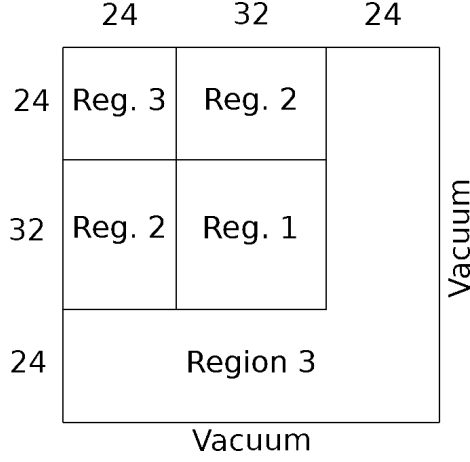


Figure 8: Geometrical model of 1/4 reactor core TWIGL-2D.

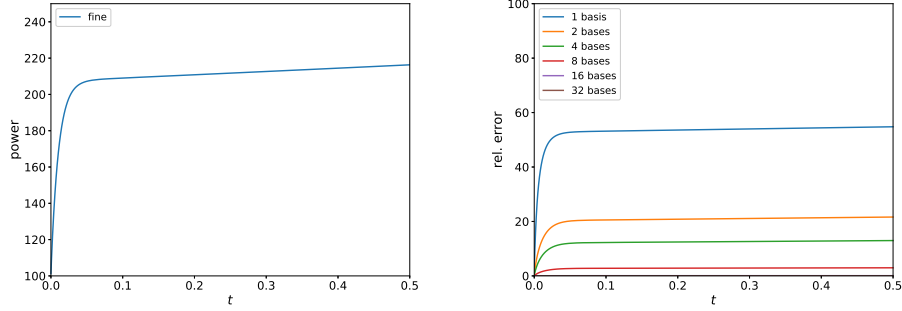


Figure 9: Integral power (fine grid) and relative errors (%) of the multiscale solution power.

## 5. Conclusions

A Generalized Multiscale Finite Element method was developed successfully for modelling neutron transport in one-group  $SP_3$  approximation. We presented an implementation of GMSFEM. We considered each step of GMSFEM algorithm. The results showed that GMSFEM performed with a good accuracy in all considered cases.

In the current work, we considered a popular and simple model of neutron transport equation. Computational expenses are always an issue even for modern computers. In the future, we will consider more complex models of neutron transport, such as  $P_N$  approximation.

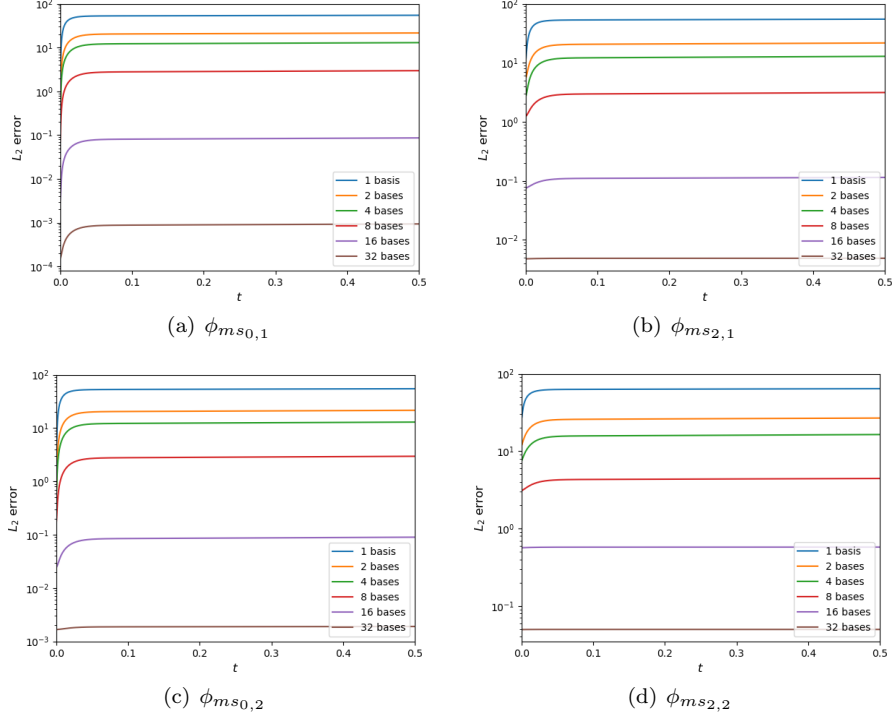


Figure 10: Relative  $L_2$  errors (%) of the multiscale solution

Table 4: Relative  $L_2$  errors (%) of the solution at final time.

Bases	DOF	$L_2$ error				Calc time
		$\phi_{ms0,1}$	$\phi_{ms2,1}$	$\phi_{ms0,2}$	$\phi_{ms2,2}$	
1	49	99.97	99.99	99.97	99.99	0.03
2	98	99.83	99.90	99.84	99.90	0.05
4	196	25.61	34.38	26.65	27.64	0.10
8	392	2.64	8.99	2.80	4.65	0.35
16	784	0.71	4.34	0.81	2.56	1.15
32	1568	0.07	1.28	0.14	1.17	6.66
fine	115891	—	—	—	—	815.00

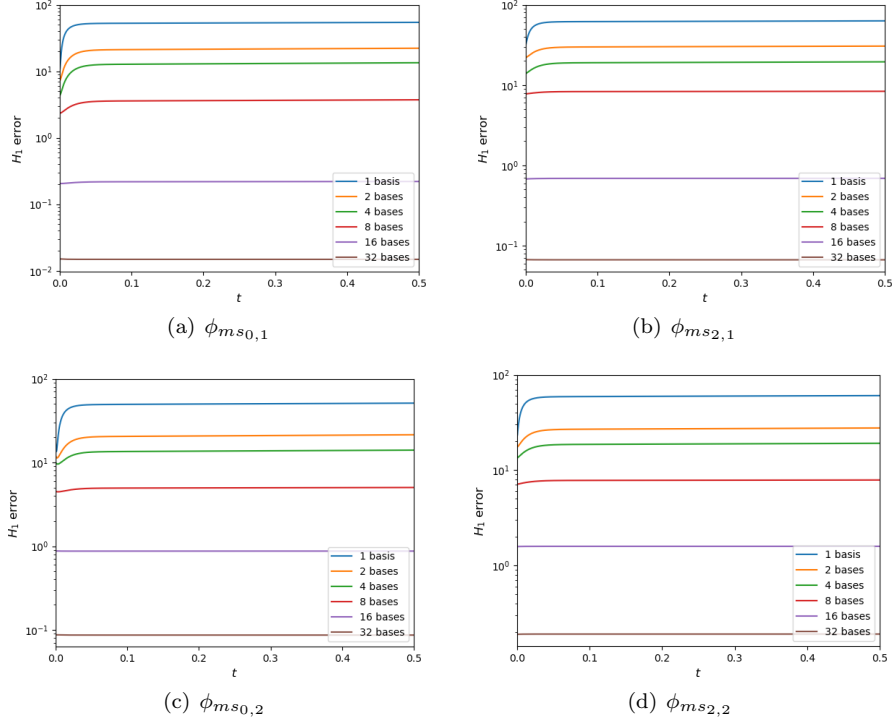


Figure 11: Relative  $H_1$  errors (%) of the multiscale solution

Table 5: Relative  $H_1$  errors (%) of the solution at final time.

Bases	DOF	$H_1$ error				Calc time
		$\phi_{ms0,1}$	$\phi_{ms2,1}$	$\phi_{ms0,2}$	$\phi_{ms2,2}$	
1	49	99.97	99.99	99.97	99.99	0.03
2	98	99.83	99.90	99.84	99.90	0.05
4	196	25.61	34.38	26.65	27.64	0.10
8	392	2.64	8.99	2.80	4.65	0.35
16	784	0.71	4.34	0.81	2.56	1.15
32	1568	0.07	1.28	0.14	1.17	6.66
fine	115891	—	—	—	—	815.00

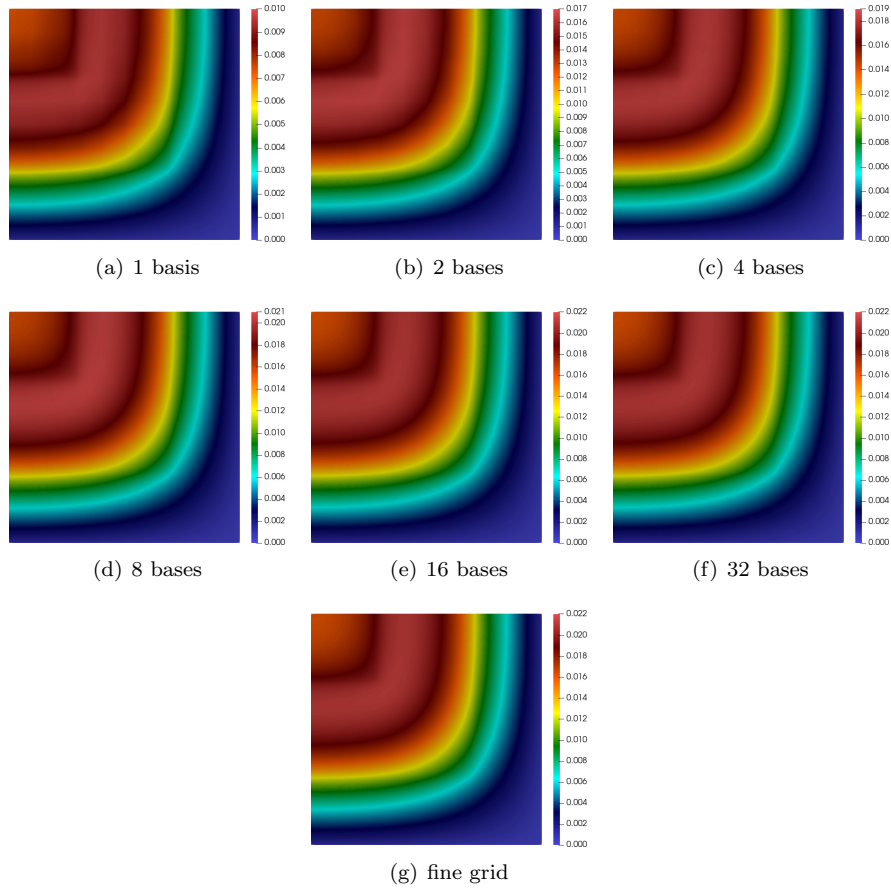


Figure 12: Fine-grid and multiscale solutions at final time for pseudo 0th moment of angular flux